Ultra-Stretchable and Superhydrophobic Textile-Based Bioelectrodes for Robust Self-Cleaning and Personal Health Monitoring

Jiancheng Dong[a], Dan Wang[a], Yidong Peng[a], Chao Zhang[b], Feili Lai[c], Guanjie He[d], Piming Ma[a], Weifu Dong[a], Yunpeng Huang[a,], Ivan P. Parkin[d,]*, Tianxi Liu[a,]**

[a] Key Laboratory of Synthetic and Biological Colloids, Ministry of Education, School of Chemical and Material Engineering, Jiangnan University, Wuxi, 214122, China

[b] State Key Laboratory for Modification of Chemical Fibers and Polymer Materials, College of Materials Science and Engineering, Donghua University, Shanghai, 201620, China

[c] Department of Chemistry, KU Leuven, Celestijnenlaan 200F, Leuven 3001, Belgium

[d] Christopher Ingold Laboratory, Department of Chemistry, University College London, 20 Gordon Street, London WC1H 0AJ, UK

* Corresponding authors
E-mail: i.p.parkin@ucl.ac.uk (I. P. Parkin), hypjnu@jiangnan.edu.cn (Y. P. Huang), txliu@jiangnan.edu.cn (T. X. Liu)

ABSTRACT

The rapid advancement of smart electronics has stimulated immense research interest in non-metallic bioelectrodes with scalable yet cost-effective fabrication, harsh-environment resistance, and superior sensing capabilities to various physiological signals. Here, an ultra-stretchable and self-cleaning nonwoven textile-based bioelectrode combining prominent health monitoring performance with outstanding anti-fouling ability is rationally designed and successfully fabricated *via* the synergistic combination of carbon black nanoparticle/CNT (CB/CNT) stretchable conductive networks and superhydrophobic perfluorooctyltriethoxysilane modified TiO_2

nanoparticles (PFOTES-TiO_2 NPs). The adaptive CB/CNT conductive networks on elastic fibers can facilitate efficient charge transfer under ultra-high deformation (>10 times stretching), while the outermost PFOTES-TiO_2 NPs layer with good interlayer adhesion provides the micro-topological structure and low surface energy. As a result, the conductive textile used as skin-attachable bioelectrode manifests remarkable performance for personal health monitoring, including an ultra-broad detection range of 1050.0% and an extremely high GF value up to 1134.7 as wearable strain sensor, and outstanding detection ability to electrocardiogram (ECG) and electromyography (EMG) signals. Moreover, the bioelectrode also possesses terrific anti-fouling properties and resistance to various corrosive fluids and even severe mechanical damage, ensuring its long-term operation stability under harsh environments. Hence, this research provides a new paradigm for achieving high-performance textile-based bioelectronics.

Keywords: textile bioelectrode, multifunction, high stretchability, self-cleaning, health monitoring

1. Introduction

The advent of stretchable electronics has yielded infinite varieties for their potent penetration into numerous areas of smart electronics such as health monitors [1-4] and artificial e-skin [5-7]. Concurrently, great challenges on flexible electronics are engendered along with the fast-growing demands on more advanced functionality, such as superior mechanical deformability [8-10], good wearing comfort to satisfy

diversified application scenarios [11-13]. As a key role in flexible and wearable electronics, stress/strain sensors can covert external physical stimuli into electrical signals, which must possess low Young's modulus and large GF value to monitor subtle skin motions, high stretchability to adapt to multi-scale deformations, and extreme durability to fit for dynamic deformations induced by human movements [14,15]. Due to these concerns, commercial brittle strain gauges are far from satisfactory in wearing devices. Thus, incorporating advanced conductive nanomaterials with stretchable supporting substrates is a versatile approach to obtain stretchable conductors for flexible strain sensors [16-19]. For example, silver nanoparticle was filled in PDMS to fabricate a stretchable strain sensor with a maximum GF value of 268.4 at 110% strain [20]. A step further, by constructing hierarchical microstructure on piezoresistive layers and introducing regulatory resistors into circuit designs, researchers also achieved a strain sensor with ultra-high sensitivity (GF≥14000) as well as a wide workable window (130% to 900%) [21]. Nevertheless, the consumption of costly conductive nanomaterials largely hinders the promotion of such strain sensors in consumer markets. In this regard, Cui *et al*. reported a low-cost strain sensing material *via* embedding inexpensive carbon nanotubes into highly stretchable styrene-ethylene-butylene-styrene (SEBS, elongation at break 940 ± 42%), yielding a sensing range of 120% and a GF value of 71.76 [22]. Another cost-effective approach was filling carbon black in commercially available rubber substrate, obtaining a highly sensitive (GF = 242.6) strain sensor with a workable range up to 71.4% [23]. However, the above strategies always confront the difficulties of dispersion, and the balance between percolation

threshold and mechanical properties. Apart from these, to fulfill practical applications in daily life and harsh environments, wearable strain sensors should be contaminant-repellent, intact to atmospheric environments, and chemically resistant to sweating and even corrosive liquids [24].

Until now, many efforts have been devoted to the development of wearable sensory devices combining high sensitivity and multi-functionality. Amongst, endowing sensing materials with excellent superhydrophobic surfaces is identified as an accessible and potent approach to realize anti-fouling and anti-corrosion capabilities. However, there are scarcely any elastomeric substrates that possess complete waterproof surfaces due to their intrinsic molecular structures. To overcome this deficiency, many scientific endeavors have been directed toward constructing surface micro-/nano-structures and utilizing low surface energy strategy to fabricate superhydrophobic and anti-fouling strain sensors [25-29]. For instance, waterproof nonwoven fabric-based conductors were prepared using cellulose nanocrystal, graphene, and fumed silica to construct micro-cracked conductive layer and nanoscale surface topography [30]. Another PDMS film-based superhydrophobic strain sensor equipped with a water repellency surface was developed *via* forming silica nanoparticles microcilia architecture on the matrix [31]. Though both sensors presented desirable superhydrophobic capabilities, they still suffered from limited strain sensing performance and severe moisture impermeability, thus can hardly satisfy practical applications in wearable and stretchable electronic devices.

Given the aforementioned challenges, herein, a cost-effective nonwoven textile-based bioelectrode with skin-like Young's modulus, ultra-high stretchability, superhydrophobicity, as well as remarkable strain sensing and bioelectric detection performance is successfully fabricated *via* evenly anchoring CB/CNT hybrids onto electrospun SEBS nonwoven textiles, followed by uniformly spraying PFOTES-TiO_2 NPs on top of the conducting layer (**Fig. 1**). The stretchable conductive layer tightly incorporated on the SEBS fibers endows the composite elastomeric textiles with quick and stable sensing response to large deformations, meanwhile, micro-topological structure and low surface energy contributed by the PFOTES-TiO_2 layer successfully renders the textile-based bioelectrode with outstanding water repellency. As a consequence, an ultra-broad detection range of 1050.0% and an extremely high GF value up to 1134.7 are synchronously achieved when the conductive nonwoven textile is applied as a wearable strain sensor. Moreover, accurate and stable ECG and EMG signals can be efficiently monitored when the conductor is used as physiological electrical sensor. What's more, the composite nonwoven textile even exhibits robust anti-fouling property and excellent resistance to salty water, alkali, and acid solution. It is envisioned that the presented cost-effective textile bioelectrode can be widely adopted in skin-attachable bioelectronics applied in harsh and underwater environments.

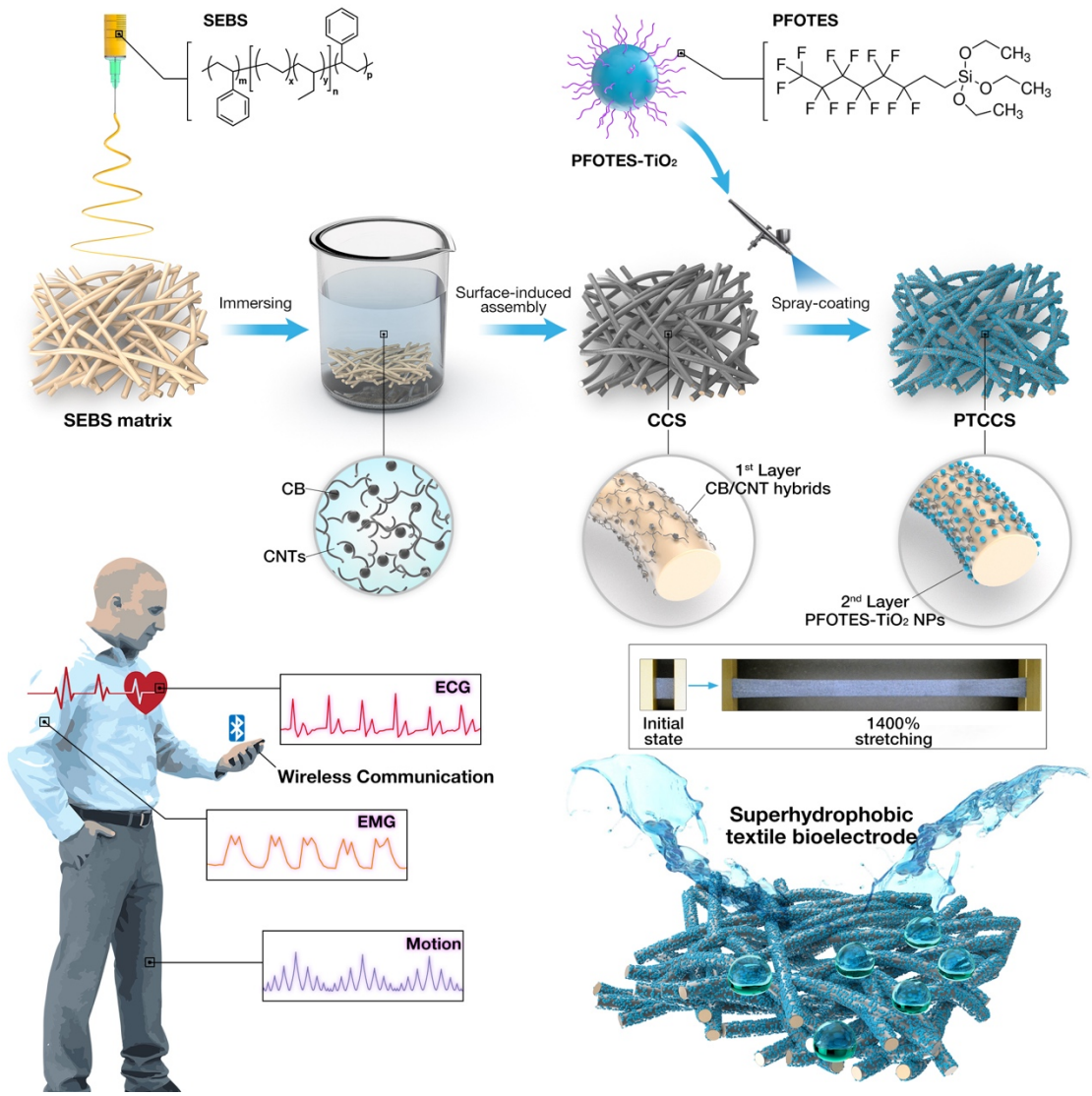

Fig. 1. The entire fabrication process of the ultra-stretchable and superhydrophobic textile-based bioelectrode.

2. Experimental section

2.1. Materials

Styrene-ethylene-butylene-styrene (Kraton G1633) was obtained from Kraton. Poloxamer (F127, 12600 g mol^{-1}) was supplied by Sigma-Aldrich. Carbon black (CB, XC-72, particle size: ~30 nm) was bought from Carbot, carboxylated multiwall carbon

nanotubes (CNTs, carboxyl contents: 0.73 wt.%, length <10 μm, outer diameter: 30-50 nm) were purchased from Chengdu Organic Chemicals Co., Ltd. Commercial dispersants (XFZ20) were obtained from Nanjing XFNANO. Perfluorooctyltriethoxysilane (PFOTES) was purchased from Beijing Innochem. TiO_2 P25 was supplied by Degussa. Common laboratory solvents were all obtained from Sinopharm Co., Ltd.

2.2. Fabrication of SEBS nonwoven textiles

SEBS masterbatch and auxiliary spinning reagent F127 (10 wt.% of SEBS) were first dissolved in a mixed solvent of $CHCl_3/CH_3C_6H_5$ (90/10 wt.%) with a total mass fraction of 15 wt.%. The above solution was vigorously stirred for 3 h, then transferred to an electrospinning apparatus with the process parameters listed as follows: injection speed was kept at 10 mL h^{-1} through an 18 G syringe needle, applied positive voltage and negative voltage was 30 kV and -1.5 kV, respectively, distance from orifice to drum receiver was 15 cm, and a constant rotating speed of the drum was kept at 80 rpm. The whole electrospinning process was carried out in a sealed chamber with a constant temperature of 35°C and a relative humidity of 30%.

2.3. Preparation of CB/CNT/SEBS textile-based bioelectrodes

Typically, 1 g CB and 1 g CNTs were respectively added in 200 mL deionized water containing 200 mg dispersant (XFZ20), followed by probe sonication (800 W) intermittently for 60 min in the ice bath. The obtained CB and CNTs suspensions were

then mixed in volume ratios of 25/75, 50/50, and 75/25, respectively, followed by another process of probe sonicating for 60 min to obtain different CB/CNT hybrid suspension. Electrospun SEBS nonwoven textiles with an average thickness of 200 μm were cut into pieces with the size of 40 × 40 mm^2, which were then immersed in the above carbonaceous dispersion for 10 min in the ultrasonic bath for the assembly of CB/CNT hybrids. After that, the wet textiles were vacuum dried at 60°C for 6 h, resulted black products were termed as CCS-25/75, CCS-50/50, and CCS-75/25 respectively.

2.4. Incorporation of PFOTES-TiO_2 superhydrophobic layer

The fabrication process of PFOTES-TiO_2 NPs incorporated CCS textile conductor (denoted as PTCCS) is schematically depicted in Fig. 1A. 1 g PFOTES was dissolved in 99 g dry ethanol under vigorous stirring for 2 hours. After that, 10 g Degussa P25 TiO_2 was added to the above solution to get a paint-like suspension. Following that, 4 g of above freshly-prepared suspension was transferred to an air-brush and sprayed (30 psi) onto both sides of the CCS textile (5×5 cm^2), which was dried in air to obtain the superhydrophobic layer enhanced PTCCS textile-based bioelectrodes as shown in Fig. S1 (total PFOTES-TiO_2 NPs content: 16 mg cm^{-2}).

2.5. Characterizations and measurements

Transmission electron microscopy (TEM) images were captured utilizing a JEM-2100plus microscope at a beam acceleration of 200 kV. Fiber morphologies were

observed by the Hitachi-S480 field emission scanning electron microscope (SEM). Elemental distribution on the samples was scanned by EDS. X-ray photoelectron spectroscopy (XPS) was conducted by Axis supra (Kratos) photoelectron spectrometer with monochromatic Al-Kα source to identify the chemical constituents. Raman spectra were acquired using Renishaw inVia Reflex spectrometer irradiated at 532 nm laser. Contact angle measurements were carried out on OCA15EC Dataphysics. Tensile tests were measured with a universal UTM2203 tensile testing machine (Sun Technology Co., Ltd.). The electromechanical properties of bioelectrodes were investigated using a Mark-10 force tester coupled with a Keysight 34465A digital multimeter.

3. Results and discussion

3.1. Structural and morphological characterization

Fig. 1 illustrates the entire fabrication process of PFOTES-TiO_2 treated CB/CNT/SEBS nonwoven textiles. As shown in Fig. S2, pristine SEBS fibers produced by electrospinning exhibit poor hydrophilic properties with a water contact angle (WCA) of 136.2°. To realize the accessibility and complete penetration of the CB/CNT hybrids into the porous fiber networks, auxiliary spinning reagent F127 was incorporated in the SEBS matrix to hydrophilize the elastomer fibers. The obtained F127 blended SEBS textile manifests web-like morphology with smooth fibers randomly connected with each other, which shows a WCA of about 42.9° (Fig. S3), demonstrating the successful hydrophilization of electrospun SEBS substrates. Notably, the fibre diameter of SEBS fibers significantly decreases from 14.9 μm to 6.3 μm after

blending with F127 (Fig. S2C and 2D), the finer fiber diameter can effectively increase the specific area of the film, which is beneficial for the subsequent combination with the conductive nanomaterials. Besides, the F127 blended SEBS fiber film exhibits extremely high stretchability with a striking 1400% elongation (inset of Fig. 1, detailed mechanical characterization will be discussed in the next part). All-carbon CB/CNT hybrids were prepared with the help of XFZ20 dispersant through the strong interfacial interaction between two nanomaterials. In this way, 0D CB nanoparticles and 1D CNTs can form a homogeneous suspension, which remains stable after static preservation for about 30 days (Fig. S4). TEM image of the CB/CNT hybrids reveals that the long-tubular CNTs bridged grape-shaped CB nanoparticles (~30 nm) are compactly interlacing and well-proportioned distributing without obvious aggregation (Fig. S5).

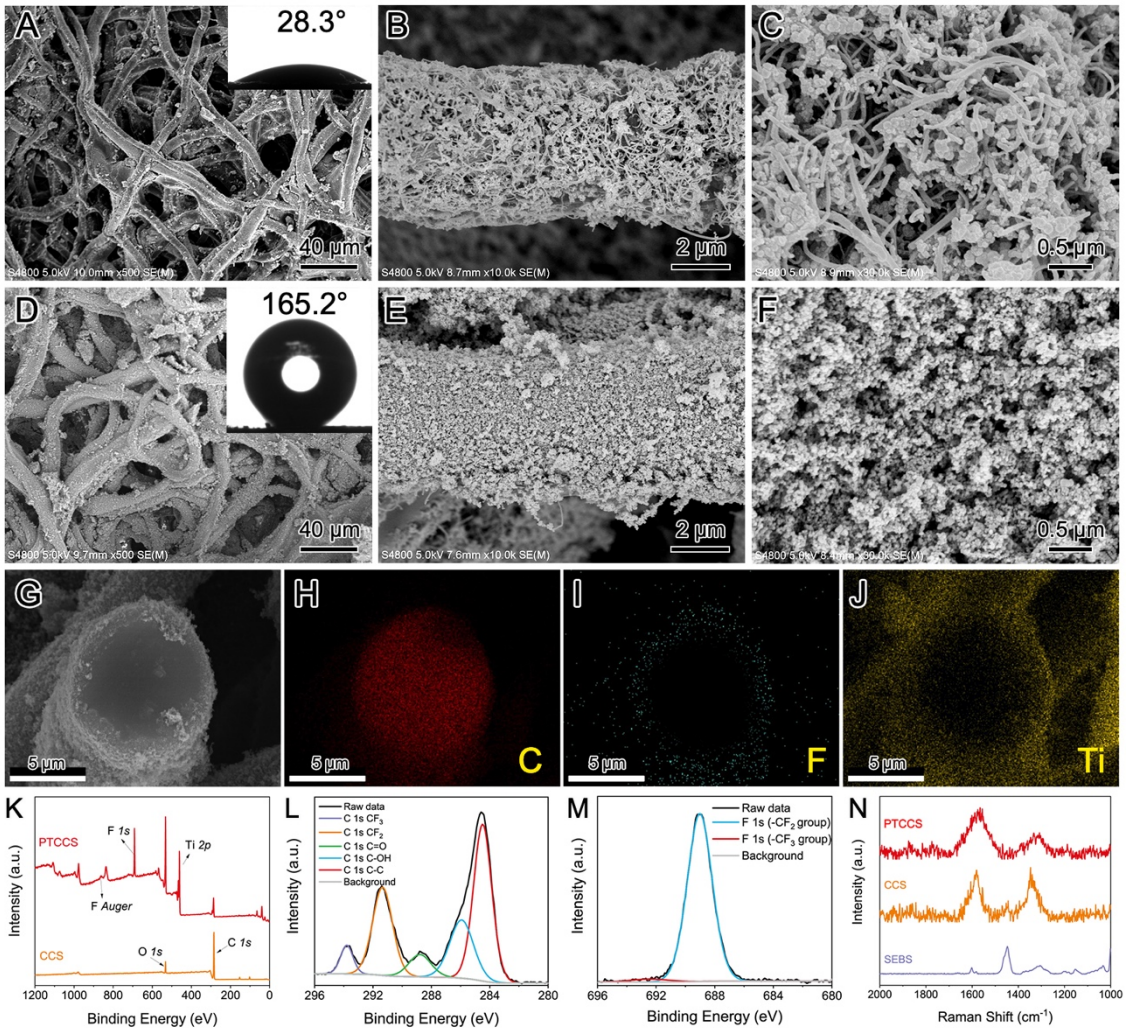

Fig. 2. SEM images of different samples at various magnifications: (A-C) CCS conductor (inset of A shows the water contact angle is 28.3°). (D-E) Superhydrophobic PTCCS textile (inset of D shows the water contact angle is 165.2°). (G-J) Elemental mapping on the cross-section of PTCCS fibre. (K-M) XPS survey spectra of CCS and PTCCS, and corresponding high-resolution spectra of C1s and F 1s in PTCCS. (N) Raman shifts of SEBS, CCS and PTCCS.

After a versatile dip-coating process, CB/CNT hybrids can be easily incorporated with the hydrophilize SEBS nonwoven textiles. As shown in Fig. S6, the color of the

elastomer fibre film changes from pure white to uniform black and finally dark grey, a careful inspection under microscope discloses that the CCS fiber surface is evenly and densely coated with CB/CNT hybrids (**Fig. 2**A and 2B), the microporous structure of the fiber film is entirely inherited without the existence of any blocking and aggregation. Additionally, high magnification SEM image indicates CB and CNTs are homogeneously mixed after depositing on the SEBS matrix (Fig. 2C), the 0D CB particles filled in the voids of 1D CNTs can function as bridges to improve the stretchability of the hybrid conducting layer, thus potentially enlarges the working range of the CCS textile-based strain sensor. Notably, the elastomeric textile remains hydrophilic (WCA = 28.3°) after coating the CB/CNT hybrids (inset of Fig. 2A), which is ascribed to the oxygen-containing groups on CB and CNTs particles. CB/CNT hybrids with other mixing ratios were also incorporated with the SEBS fiber matrix to optimize the overall performance of the textile bioelectrodes. As illustrated in Fig. S7A and S7B, CB/CNT hybrids in volume ratios of 50/50 and 75/25 also manifest high mixing uniformity, which are all evenly coated onto the SEBS fibers (Fig. S7C and S7D). Furthermore, to render the conductive CCS textiles with water repellency and anti-fouling capability, hierarchical micro-topological structures were constructed on top of the CB/CNT hybrid layer utilizing PFOTES treated TiO_2 nanoparticles (PFOTES-TiO_2 NPs). As revealed in Fig. S8, spherical TiO_2 shows a narrow size distribution with a mean diameter of ~25 nm. PFOTES possesses bifunctional groups (R-SiO_3 and R-F, as shown in Fig. 1) and high penetrability, which can greatly decrease the surface energy of TiO_2 to effectively establish a waterproof surface. *Via* a simple

yet versatile spray coating strategy, PFOTES-TiO_2 NPs can be evenly and tightly immobilized on the CCS fiber surface (Fig. 2D-2F), resulting in a surface with robust nano-topography and remarkable hydrophobicity (WCA = 165.2°, inset of Fig. 2D). It is also obvious that the CB/CNT hybrid nanoparticles are completely covered by PFOTES-TiO_2 NPs, indicating the high efficiency of spray coating and the high affinity between two layers. An EDS scan on the cross-section of PFOTES-TiO_2 coated CCS fibers (PTCCS) discloses the well-defined distribution of C, F, and Ti elements on the fringe of the cross-section, confirming the homogeneous coating of PFOTES on the outer surface.

Successful modification of PFOTES-TiO_2 NPs is also proved by XRD that the diffraction peaks of PTCCS conform to the expected patterns of anatase TiO_2 (Fig. S9A) [28]. The absence of the diffraction peak of amorphous carbon is due to the dense coating of TiO_2 NPs and their high diffraction intensity. The compositional information of PTCCS composite film was further investigated *via* XPS analysis. From the survey spectrum (Fig. 2K), C, F, and Ti signals can be clearly detected. As for the C 1s spectrum (Fig. 2L), it is found that the main peaks can be divided into five peaks: -CF_3 (293.8 eV), -CF_2 (291.35 eV), -C=O (288.78 eV), C-OH (285.93 eV) and C-C (284.52 eV) [32,33]. In the F 1s spectrum (Fig. 2M), a small shoulder peak at 692.6 eV is attributed to the -CF_3 group while the main peak located at 689.1 eV corresponds to the -CF_2 group [28]. The spectrum of Ti 2p presents the Ti 2p 1/2 at 464.9 eV and the Ti 2p 3/2 located at 459.2 eV (Fig. S9B). The XPS results clearly demonstrate the existence of -CF_2 and -CF_3 groups on the surface of PFOTES-TiO_2 NPs [28,34], which

play key roles in the superhydrophobicity of the conductive textile. Raman shifts provide fingerprints of SEBS and reinforced SEBS fibres (Fig. 2N). The =C-H and -C=CH stretching of styrene segments of SEBS can be observed at 1605 cm^{-1}, 1004 cm^{-1}, and 623 cm^{-1} [35]. Furthermore, C-H vibrations located at 1153 cm^{-1} and 1001 cm^{-1} can be ascribed to the elastic portion (ethylene-butylene) of SEBS [36]. Raman bands at 1581 cm^{-1} and 1346 cm^{-1} in the spectrum of CCS demonstrate the successful coating of CB/CNT hybrids [37]. Notably, PFOTES-TiO_2 anchoring shows neglectable influence on the Raman spectrum of the nonwoven textile, indicating the good stability of the CB/CNT conductive layer.

3.2. Mechanical properties

SEBS is composed of soft segments of polyethylene and polybutylene, and hard segments of polystyrene, strong phase separation exists in the chain of SEBS because the elastic portions and hard polystyrene are thermodynamically incompatible, resulting in the formation of polystyrene domains (**Fig. 3**A) [38-40]. These domains act as physical crosses similar to the disulfide bonds in vulcanized rubber. As is widely known, reliable mechanical properties are indispensable for flexible and wearable electronics, which greatly affect their practical applicability. As depicted in Fig. 3B, pristine SEBS substrate exhibits relatively higher tensile strength (0.86 MPa) and toughness (4.07 MJ m^{-3}) than that of SEBS with F127 additive (0.48 MPa, 3.29 MJ m^{-3}). However, the incorporation of F127 significantly increases the stretchability of the nonwoven SEBS textile to 1402.6%, despite the remarkable improvement in hydrophilicity as mentioned

above. The Young's modulus of F127 blended SEBS film is also reduced from 46.7 kPa to 28.9 kPa. A low Young's modulus normally means the material could be deformed by a certain stress very easily, flexible strain sensors with low Young's modulus are highly desirable to detect small human motions, especially subtle deformations such as wrist pulse and phonation. More importantly, the Young's modulus value is also very close to the value of human skin (<25 kPa), making it a highly suitable substrate for the fabrication of "skin-like" and "unfeelable" wearing devices [41,42].

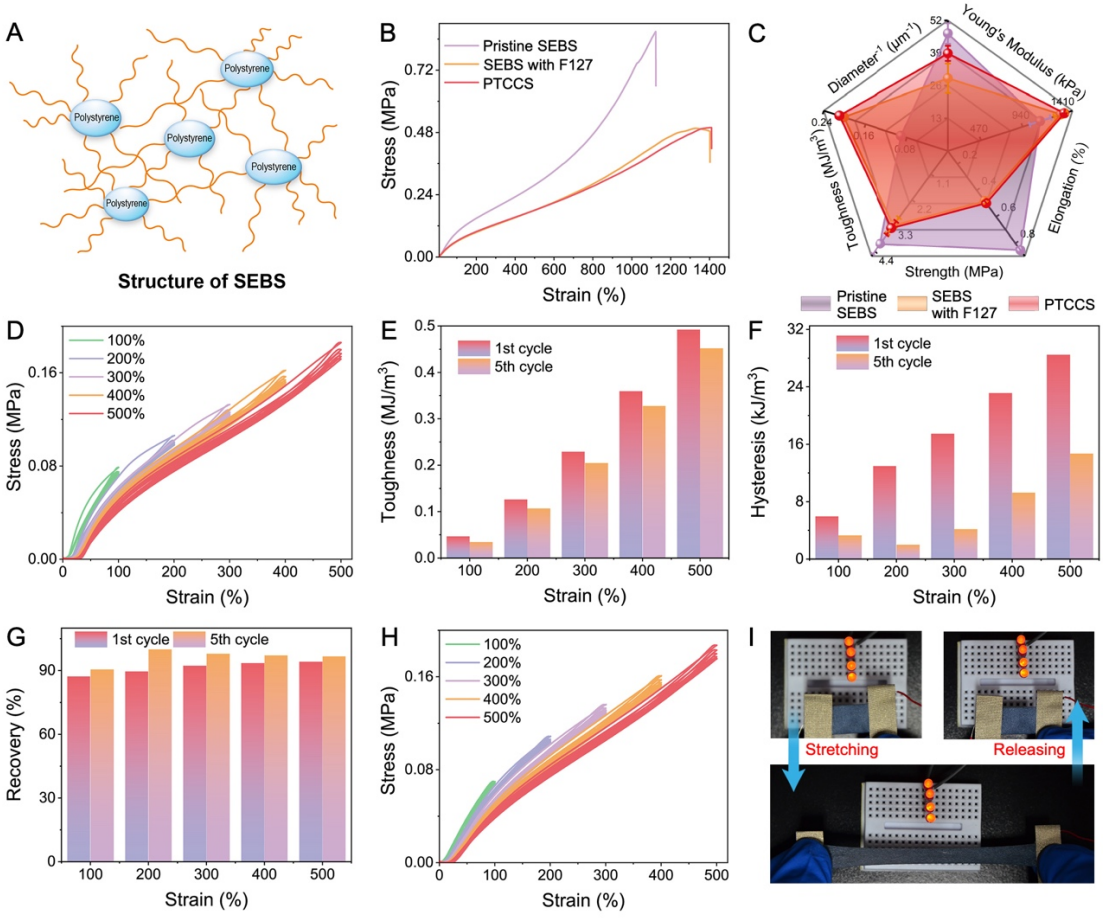

Fig. 3. (A) Structure of SEBS. (B) Strain-stress curves and (C) comprehensive mechanical properties of pristine SEBS, SEBS with F127 additive, and PTCCS textile.

(D) Strain-stress curves of hydrophilized SEBS substrates under varied elongations from 100%~500% for five cycles, and the corresponding (E) toughness, (F) hysteresis, and (G) recovery rates of the first and fifth cycles. (H) Strain-stress curves of PTCCS nonwoven textile with strains from 100%~500% for five cycles. (I) Digital photographs showing the electrical conductivity of the PTCCS bioelectrodes under stretching and releasing.

To satisfy the long-term and stable response of the strain sensors, high toughness and great resilience of the elastic substrate are imperative. A series of cyclic stretching-releasing tests were conducted to explore the toughness and the resilience of the elastomeric textiles. Fig. 3D-3G displays the hysteresis loops and corresponding toughness, hysteresis, and recovery of F127 blended SEBS film under strains from 100% to 500% in five cycles. Different from frequently utilized elastomers like TPU [43], electrospun SEBS nonwoven textile shows very limited hysteresis and neglectable hysteresis loops, even under large deformations beyond 200%. Notably, the releasing curve tends to overlap with the previous stretching curve, implying the elastomer may undergo a self-recovery process upon releasing. The slight decrease of the toughness in the fifth cycle could be ascribed to the energy dissipation from the frictions of highly entangled molecular chains (Fig. 3A) and reconstruction during the repeated large deformations [44]. Additionally, elastic matrix with lower hysteresis always exhibits better resilience [45], as demonstrated in Fig. 3G and Fig. S10, prepared SEBS fibre film displays outstanding resilience with very low hysteresis even under 500%

elongation. In brief, the high toughness and excellent resilience of SEBS nonwoven textile can be attributed to the efficient energy dissipating by destroying the physical cross-links during stretching [46,47], thus making the F127 blended SEBS elastic matrix an ideal substrate for flexible sensors. Furthermore, mechanical properties of the fibre film almost show no change after successive coating of CB/CNT hybrids and PFOTES-TiO_2 NPs (Fig. 3B, Fig. 3C and 3H), manifesting the good stability of the SEBS matrix. Fig. 3I demonstrates that the fabricated PTCCS exhibits fabulous electrical conductivity under extremely large deformation, revealing the great potential of the textile conductor in stretchable sensing devices.

3.3. Superhydrophobic and self-cleaning performance

Flexible strain sensors with the advantages of anti-fouling, self-cleaning, and anti-corrosive abilities are highly preferable for the routine use of wearable electronics. Artificial self-cleaning materials usually work through extreme water repellent surfaces, where water droplets can form approximate spherical shapes to pick up and erase dust, bacteria, and even viruses during the rolling motion [48]. To obtain near-spherical water droplets, the surfaces must be highly textured and with extremely low water affinity. In this work, a robust superhydrophobic layer on CCS nonwoven conductor was realized *via* the facile spray coating of PFOTES-TiO_2 NPs, the obtained PTCCS composite film becomes completely waterproof with a WCA up to 165.2° (Fig. 2D). Besides, PFOTES and TiO_2 nanoparticles were respectively applied for the surface treatment of CCS film *via* the same spray coating. As illustrated in Fig. S11, the CCS fibre films treated with

PFOTES and TiO_2 manifest completely different wetting behaviors with WCAs of 112.8° and 12.6°, indicating the superhydrophobicity of PTCCS nonwoven textile is owing to the synergistic contributions of PFOTES and TiO_2 nanoparticle [25]. The superhydrophobicity of PTCCS textile-based conductor was evaluated by immersing it in dyed water, which stays completely dry after being taken out from the beaker (Fig. S12A). Contrarily, the untreated CCS sample gets completely wetted under the same circumstances (Fig. S12B). What is more, PTCCS nonwoven textile shows great repellency ability to various liquids, including coffee, cola, juice, ink, yogurt, and even salty, acid, and alkali solutions. As shown in **Fig. 4**A, all liquid droplets stand on the surface with nearly spherical shapes instead of permeating into it. The WCAs of the above liquids are displayed and compared in Fig. 4B, which are all greater than 150°, revealing the outstanding liquid repellency of the PFOTES-TiO_2 NPs treated elastic conductor. Because the fabricated textile-based strain sensor is expected to be used under extremely large deformation, the stability of superhydrophobicity was carefully explored at various stretching strains. As shown in Fig. 4C, the WCA remains above 150° on PTCCS even under a high elongation of 300%, verifying the excellent stability of the superhydrophobic surface.

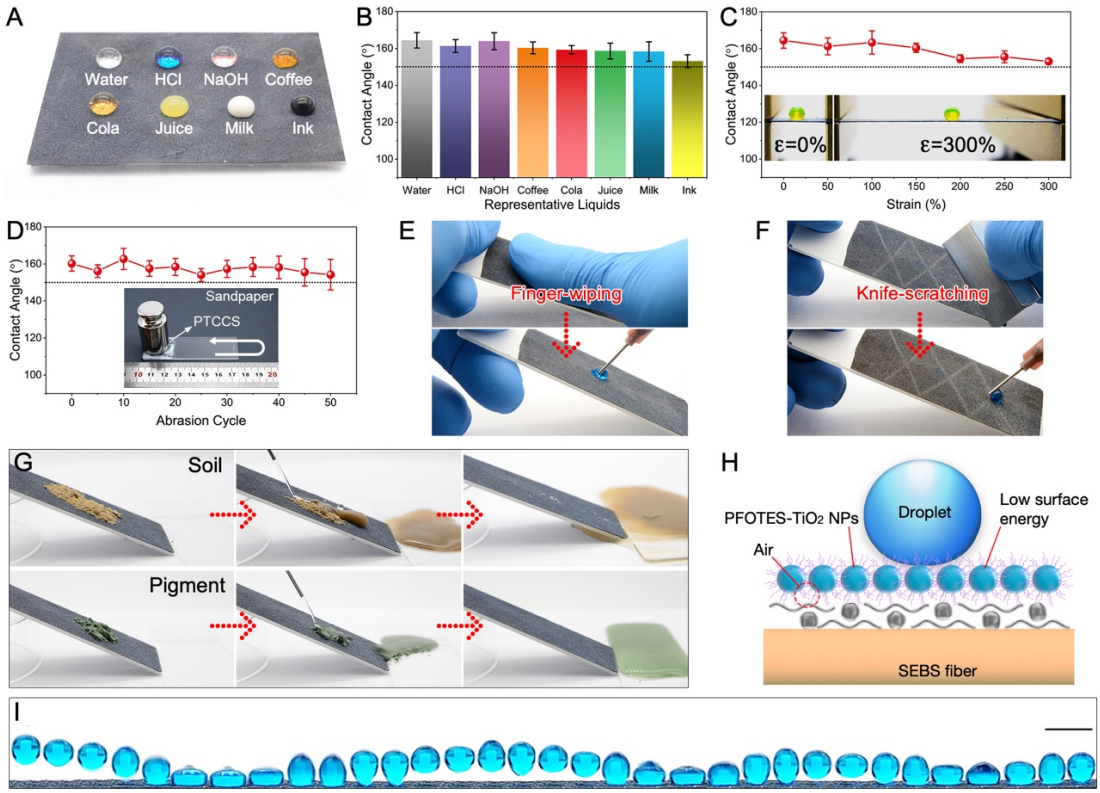

Fig. 4. (A) Digital photographs of water, HCl (1 M) solution, NaOH (1 M) solution, coffee, cola, juice, milk and ink droplets on superhydrophobic PTCCS nonwoven textile, and (B) their corresponding WCAs. (C) WCAs of PTCCS under increased strains from 0% to 300% (inset: fluorescein dyed water droplet on PTCCS textile during stretching). (D) Abrasion-resistance tests on the superhydrophobicity of PTCCS for 50 cycles (inset: a weight of 100 g on the PTCCS). Influence of mechanical damage on the superhydrophobicity of PTCCS: (E) hand-rub, and (F) knife-scratch. (G) Self-cleaning tests on PTCCS textile using water flux to remove natural soil and pigment. (H) Schematic showing the superhydrophobic surface of PTCCS. (I) A water droplet bouncing on a horizontally placed PTCCS nonwoven textile (time interval is 33 ms, scale bar: 5 mm).

Furthermore, wearable devices ought to be stable in complex and harsh environments, so the stability and durability tests on the superhydrophobicity of PTCCS were also performed under mechanical abrasion, knife-scratching, and chemical corrosion. Mechanical destruction is one of the most challenging obstacles that deteriorates superhydrophobic properties. At first, a sandpaper abrasion test was conducted to assess the stability of the water-proof surface against mechanical wear. In this research, the PTCCS textile under a weight of 100 g (8 kPa) was abraded by 1200 grid SiC sandpaper and moved for 10 cm as a cycle. The WCA was measured after every 5 abrasion cycles. As shown in Fig. 4D, the WCA slightly decreased from 162° to 152° after 50 cycles (the total abrasion distance is about 5 m), indicating the constructed superhydrophobic layer is perfectly maintained. Then, hand-rubbing and knife-scratching tests were further imposed on the PTCCS (Fig. 4E and 4F). It can be observed that the water droplets roll off readily from the tortured surface after both damages are applied. The morphology of PTCCS nonwoven textile after mechanical wear was examined, no obvious microstructure damage could be observed in Fig. S13, confirming the good adhesion properties of the PFOTES-TiO_2 NPs coating [49]. Finally, the anti-corrosion ability of the PTCCS nonwoven textile was evaluated by soaking it in three typical corrosive liquids for 24 h (Fig. S14), *i.e.*, HCl solution (pH = 1), 5 wt.% NaCl, and NaOH solution (pH = 14). Interestingly, the WCAs of all samples remain greater than 150° (Fig. S14B and 14C), the surface morphology and structure are evidenced to be well preserved (Fig S13D-13F), demonstrating the outstanding chemical resistance of the fabricated superhydrophobic bioelectrodes.

Based on the excellent liquid repellency of PTCCS nonwoven textile, it also exhibits prominent self-cleaning and anti-fouling properties. As presented in Fig. 4G and Video S1, natural soil, pigment, and sticky ketchup are used as model contaminants, it is interesting that the flowing water can pick up and remove the contaminants easily and instantly to keep the film dry and clean, indicating the robust self-cleaning capability of the superhydrophobic PTCCS fiber film. Fig. 4H schematically illustrates the mechanism of the superhydrophobic surface of PFOTES-TiO_2 NPs immobilized PTCCS textile. Typically, the excellent water repellency is ascribed to the collaborative contribution of the surface roughness formed by TiO_2 nanoparticles, and the low surface energy stem from PFOTES treatment, as well as the Cassie−Baxter state which can trap air pockets to prevent droplets from penetrating [50]. Fig. 4I and Video S2 presents the time-resolved images of the bouncing of a 10 μL water droplet on the PTCCS film surface, it is exciting that the droplet can rebound repeatedly before it undergoes damped oscillations and eventually rests on the fibre film.

3.4. Strain-sensing performance

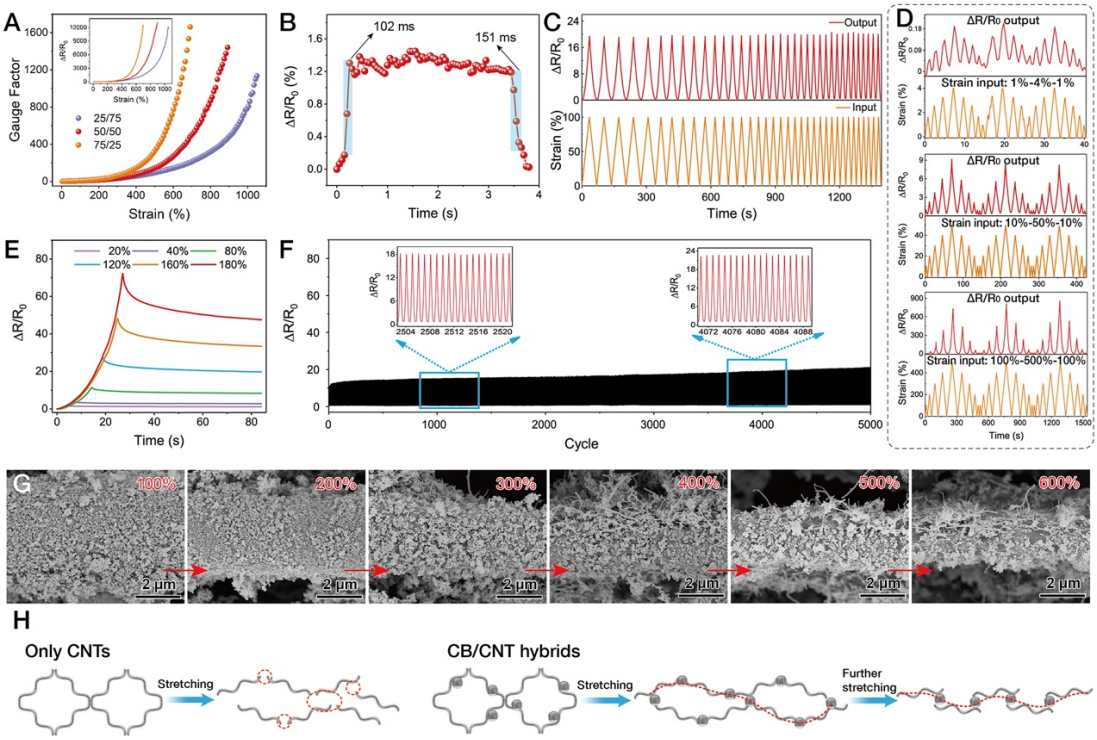

Fig. 5. (A) Plots of gauge factor versus strain of PTCCS strain sensor with CB/CNT volume ratios of 25/75, 50/50 and 75/25 (inset: plots of $\Delta R/R_0$ versus strain). (B) Response/recovery times of PTCCS strain sensor with CB/CNT volume ratios of 25/75. (C) Resistance changes of PTCCS strain sensor under 200% strain with gradient tensile speed of 50 mm min^{-1}~100 mm^{-1} min. (D) $\Delta R/R_0$ outputs of PTCCS under varied strain inputs of 1%~4%~1%, 10%~50%~10%, and 100%~500%~100%. (E) Static response of PTCCS under 20%, 40%, 80%, 120%, 160% and 180% strains and holding for 80 s. (F) Cyclic stretching tests of PTCCS conductor under 200% strain for 5000 cycles. (G) SEM images of PTCCS fiber under gradually increased strains of 100%~600%. (H) Schematic description of the stretchable conductive networks of CB/CNT hybrids.

During the past few years, expensive nanomaterials like silver nanoparticles [7] and silver nanowires [51] were frequently used to obtain highly sensitive strain sensors.

Apparently, the large consumption of costly metallic nanomaterials will severely limit the large-scale manufacture of sensory devices. Low-cost carbonaceous nanomaterials especially carbon nanotube and carbon black exhibit equally sensitive resistance response ($\Delta R/R_0$) owing to their similar dimensionalities at the nanoscale [52-54]. Herein, the strain sensing performance of the superhydrophobic PTCCS nonwoven conductor is systematically studied. To start with, the sensing properties of SEBS fiber films respectively coated with CB and CNTs (*i.e.*, CB/SEBS and CNT/SEBS) were studied. As presented in Fig. S15A, CB coated strain sensor shows a high GF of 2320 and a disproportionately low working range of 180%. Conversely, the sensing range of CNTs based strain sensor reaches as high as 1200%, while its GF value is only 790. Besides, the sensing limits of both sensors witness a big difference, which are 0.1% and 1.4% strain for CB/SEBS and CNT/SEBS (Fig. S15B and S15C), respectively. Hence, CB/CNT hybrids were utilized in this work to balance the trade-off between sensitivity and sensing range. **Fig. 5**A and Fig. S16-17 present the stretchability, sensitivity, and response time of the PTCCS strain sensor with CB/CNT ratios of 25/75, 50/50, and 75/25 (volume of dispersion), respectively. Specifically, the GF values of the sensors are linearly distributed in strain range of 0~200%, which are 7.06, 16.58 and 23.51 for different CB/CNTs volume ratios. The PTCCS strain sensor exhibits a significantly reinforced workable range (>690%) and sensitivity (GF>1130) for all samples. In addition, with the increase of CB content in the CB/CNT hybrids, the obtained strain sensors show an adjustable sensing range (from 691% to 1050%), sensitivity (GF value from 1134.7 to 1661.3), and detection limit (fluctuates between 0.14% to 0.18%).

Interestingly, there are insignificant changes in their response times (~100 ms) and recovery times (~150 ms), which is probably due to the equal conductivity and surface properties between CB and CNTs.

The comprehensive strain sensing properties of the PTCCS strain sensor with a CB/CNT volume ratio of 25/75 were systematically investigated within the range of 0~200%. As shown in Fig. 5B, the strain sensor shows very short response/recovery times of 102 ms and 151 ms, revealing the quick installation of conducting paths in CB/CNT hybrid networks. In addition, when the PTCCS conductor was stretched to 100% strain under a gradually increased tensile speed (50 $mm \cdot min^{-1}$-100 $mm \cdot min^{-1}$), stable resistance signal can be instantly generated by the strain sensor (Fig. 5C), indicating the sensing response of PTCCS is independent of the tensile frequency. The capability to respond steadily to variable-frequency and diverse strains is important for wearable strain sensors to satisfy real-time and complex deformations, especially for the monitoring of complicated human motions. As also demonstrated in Fig. 5D, when varied and repeated strains (1%~4%~1%, 10%~50%~10%, and 100%~500%~100%) were imposed on the strain sensor over a short period of time, it can instantly and accurately respond to the stimuli. The peaks of the input signals (strains) keep in line with the output signals ($\Delta R/R_0$), indicating the stable and reliable response of the strain sensor toward the complicated external stimulus. Moreover, the PTCCS sensor exhibits overshoots with a short creep recovery time under applied strains of 20%, 40%, 80%, 120%, 160%, and 180% at a stretching speed of 50 $mm \cdot min^{-1}$ and being static for 100 s (Fig. 5E). The $\Delta R/R_0$ maintains stable after the recovery of the overshoot, verifying

its reliable performance and stable conductive network in PTCCS. In addition, 5000 stretching cycles under 200% strain at a tensile rate of 100 mm min^{-1} were performed to examine the long-term durability of the PTCCS strain sensor. As shown in Fig. 5F, the $\Delta R/R_0$ value slightly rises and no obvious signal fluctuation can be observed, demonstrating the excellent long-run stability of the obtained sensor. Table S1 summarizes the comprehensive performance of recently reported strain sensors. As a result, the cost-effective and anti-fouling PTCCS strain sensor in this work achieves a highly competitive sensing performance with a broad workable range of 1050.0% and GF value up to 1134.7.

To better understand the strain sensing behavior of the PTCCS textile-based strain sensor, the dynamic evolution of the CB/CNT hybrid (volume ratio = 25/75) conductive network under various tensile strains was studied. As shown in Fig. 5G, the pristine PTCCS fiber is gradually stretched along the tensile direction, accompanied by the decrease of the fiber diameter and reduction of conductive paths. The PFOTES-TiO_2 outer layer is first observed to crack, progressively exposing the CB/CNT conducting layer, it is clear that the CB nanoparticles can bridge the long-tubular CNTs from complete isolation, by this way the conductive network can be largely maintained during the stretching process. The working mechanism of the hybrid conducting network is also schematically illustrated in Fig. 5H. During the stretching process, the destruction and reconstruction of the CB/CNT conductive network coexist. The carbonaceous nanomaterials are prone to rearrange when the adjacent nanoparticles (CB-CB, CNT-CNT, and CB-CNT) get apart with the deformation of the fiber

substrates. When the contact of CB nanoparticles is damaged to yield high GF, neighboring CNTs would move into the gaps to re-link the conductive paths, resulting in the ultra-broad workable range. Thanks to the collaborative contribution of 0D CB and 1D CNTs, fabricated PTCCS nonwoven textile with stretchable conductive networks manifests great potential in the highly sensitive detection of large deformations.

3.5. Personal health monitoring

Considering the desirable low Young's modulus (28.9 kPa) and high sensitivity of the nonwoven textile-based conductor, it can be readily attached to the skin surface to detect subtle deformations of body activities. Firstly, the PTCCS strain sensor was mounted on the wrist, chest and a surgical mask of an adult volunteer (27 years, male) to monitor the faint arterial pulse, heartbeat, and breath, respectively, all the response curves show steady and repetitive signals (**Fig. 6**A-6C). As shown in Fig. 6A, typical characteristic pulse waves, namely, systolic peak P_1, dicrotic peak P_2, and diastolic peak P_3, exist in all resistance profiles. These fine signals contain significant physiological and biomedical information for cardiovascular diseases like myocardial infraction, coronary artery disease, and arterial stiffness. The average radial augmentation index ($AI_r = P_2/P_1$, which is usually utilized to evaluate the stiffness of the arteries [55]) obtained from our data is calculated to be 54.7% for the volunteer, being in line with the reported results of a young male [56].

The high sensitivity and low detection limit of the PTCCS sensor inspire further evaluation on wearable recognition of feeding and speech motion of the Adam's apple. Herein, the conductive textile was attached to the volunteer's larynx for noninvasive and accurate monitoring of typical eating behaviors of swallowing and drinking, and phonation of three words with different syllables like "carbon", "strain", and "chem" (Fig. 6D and 6E). For the subtle laryngeal movement recognition, the patterns of feeding behaviors and word phonation exhibit characteristic profiles, meanwhile, the signal patterns are identical and reproducible during iteration. The quick and delicate response of the sensor encourages its potential applications in speaking rehabilitation, human-machine interaction, and artificial throats to assist speech-impaired people by converting throat vibrations into distinguishable signals. As the strain sensor possesses high stretchability, it could be easily mounted onto body joints (*e.g.*, knuckle, elbow, and knee) to monitor various large deformations. As shown in Fig. 6F, the bending of the finger at various bending angles (30–90°) was precisely tracked by the significant change in relative resistance. Interestingly, the sensor regains its baseline resistance very quickly, which is probably ascribed to the fast response of the CB/CNT conductive network. Besides, the motion of the elbow and knee joints were also investigated at relatively larger bending angles (Fig. 6G and 6H). As expected, identical and repeatable electrical signals are perfectly outputted, proving the potential of the sensor for practical applications. Lastly, fabricated superhydrophobic strain sensor was further utilized to monitor the finger bending motion under water. As revealed in Fig. 6I, stable resistance signals can be delivered along repetitive bending and straightening of the finger joint,

confirming the potential of the multifunctional PTCCS textile bioelectrodes in underwater applications.

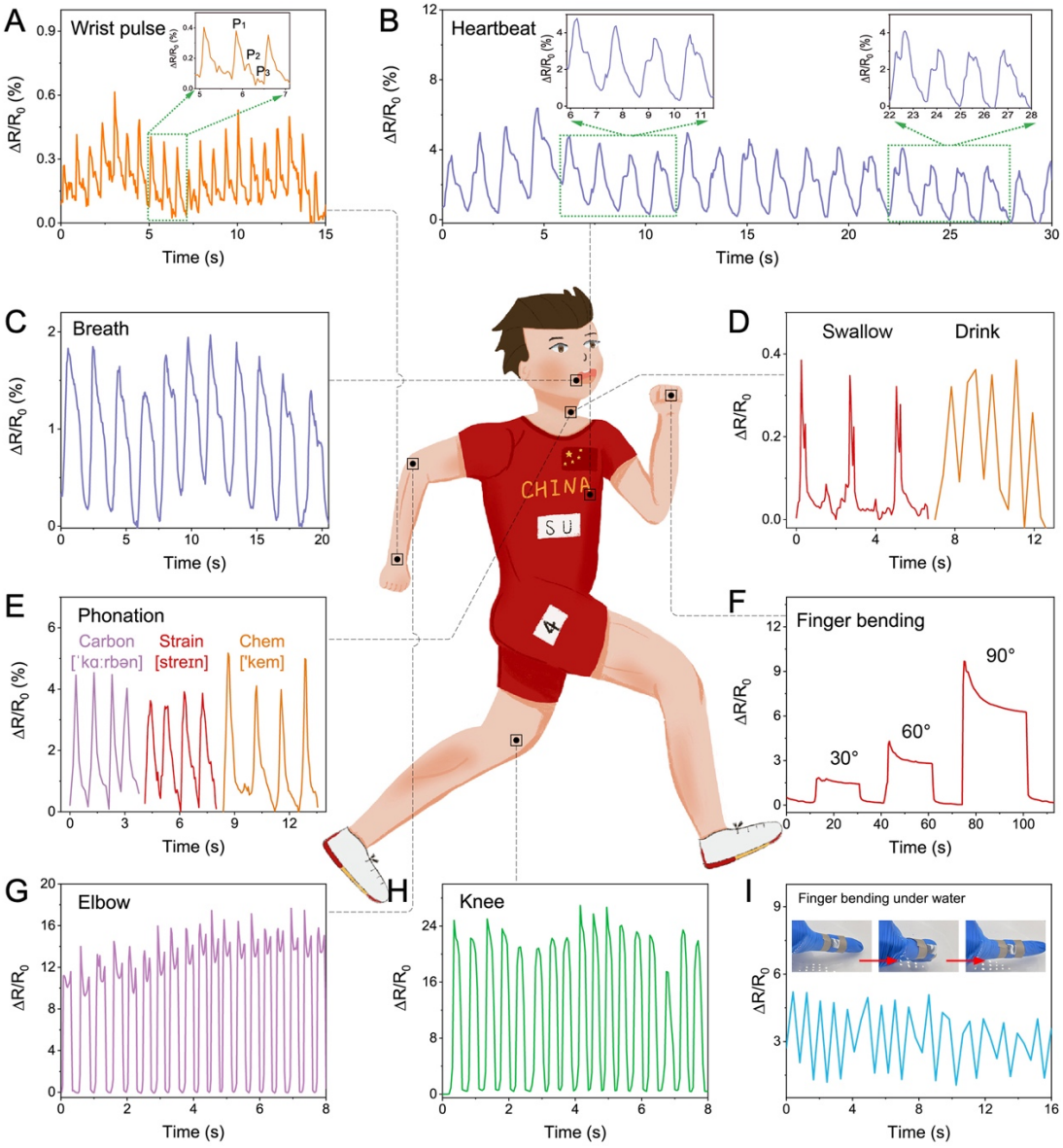

Fig. 6. Human motions detection tests: (A) wrist pulse, (B) heartbeat, (C) breath (mounted on a mask), (D) swallow and drink, (E) phonation: carbon, strain and chem, (F) finger bending for 30°, 60° and 90°, (G) elbow bending, (H) knee bending, and (I) finger bending under water.

Aside from superior strain-sensing performance, as-fabricated PTCCS textile conductor with low Young's modulus can be readily utilized as skin-adaptive bioelectrodes to replace commercial gel electrode for continuously monitoring of electrophysiological signals. In order to acquire the electrocardiograph (ECG) signals, two pieces of PTCCS electrodes were mounted onto the chest of a volunteer with a wireless ECG recorder (**Fig. 7**A). As demonstrated in Fig. 7B and Video S3, the ECG signals can be conveniently received by a smart phone *via* Bluetooth connection, facilitating its practical applications in personal health monitoring. The ECG signals before and after 30 min exercising at heart rate of 70 bpm and 120 bpm were collected using a home-made ECG device (Fig. 7C-7E). Surprisingly, PTCCS electrodes provide comparable ECG signals to commercial impermeable gel electrode, when the heart rate was 70 bpm (calm state), the amplified signals present clear P, QRS complex, and T-waveform for both electrodes. When the heart rate reached 120 bpm after 30 min of jogging, major characteristic peaks of the electrophysiological are also well recorded, revealing the superior performance of the textile electrodes. Electromyography (EMG) is the electric-potential induced by muscle contraction, which can be used to analyze muscle conditions (abnormalities, activation level, *et al*.) and the biomechanics of human movement. As shown in Fig. 7F and 7G, EMG detection device was developed on an Arduino platform, which was connected with two pieces of PTCCS textile electrodes attached to the belly of bicipital muscles (detection electrode) and the elbow joint (reference electrode). The raw EMG data was collected by a customized software where the signals were full-wave rectified and further quantified by root-mean-square

(RMS) method to transfer the analog signals to more recognizable digital signals (Video S4). As shown in Fig. 7H, positive, concise and clear EMG signals corresponding to three typical contraction motions of bicipital muscles, namely, clench, elbow raising, and forearm supination, are successfully obtained, verifying the great application prospects of the PTCCS textile conductor in bioelectric detection.

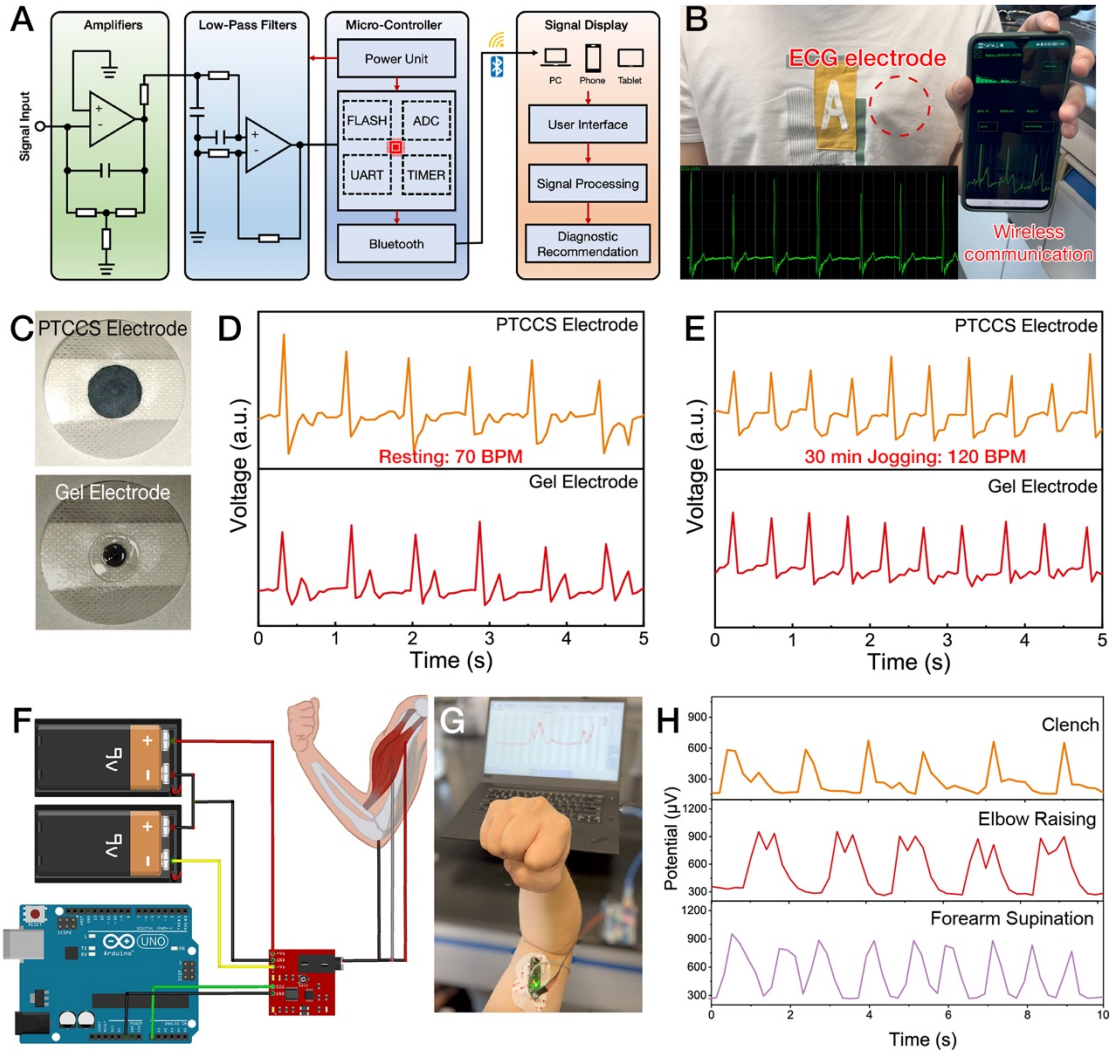

Fig. 7. (A) Schematic diagram of the PTCCS-based ECG-signal management circuit with four components of data acquisition, signal processing, and wireless transmission. (B) Real-time ECG signal displaying on a cell phone *via* Bluetooth connection. (C)

Digital photographs of the commercial gel electrode and PTCCS electrode. ECG signals measured by two electrodes (D) before and (E) after exercising. (F, G) Schematic setup and photograph of EMG device for measuring bioelectricity of bicipital muscle, and (H) acquired EMG signals of clenching, elbow raising, and forearm supination.

4. Conclusion

In summary, a low-cost nonwoven PTCCS textile-based bioelectrode with robust self-cleaning capability and ultra-high stretchability was fabricated *via* the synergistic combination of stretchable CB/CNT conductive networks and outermost superhydrophobic PFOTES-TiO_2 NPs. The CB/CNT hybrid conductive network was anchored securely on the fiber surface and facilitates efficient charge transfer under ultra-high deformation through the collaborate contribution of two nanoparticles, thus synchronously yielding a wide working range (1050.0%), a high GF value (1134.7), an ultralow sensing limit (0.18%), as well as the outstanding ability to monitor in real-time various human activities when applied as wearable strain sensors. When used as a physiological electrical sensor, the PTCCS textile bioelectrode also shows remarkable detection performance when ECG and EMG signals are recorded. Furthermore, the low surface energy combined with hierarchical nano-micro structure provided by PFOTES-TiO_2 NPs keep the surface of the textile conductor in a Cassie state, leading to robust water-repellency even after finger-wipe, knife-scratch, and abrasion with sandpaper, and most importantly, the great sensing ability under wet and corrosive environments.

Considering the diversified functions and remarkable performance of the textile bioelectrode, this work may provide new ideas to fabricate skin-attachable health monitoring electronics with harsh environment adaptability.

Declaration of Competing Interest

The authors declare that they have no known competing financial interests or personal relationships that could have appeared to influence the work reported in this paper.

Acknowledgements

This work is financially supported by the National Natural Science Foundation of China (No. 21875033), the Shanghai Scientific and Technological Innovation Project (No.18JC1410600), the Program of the Shanghai Academic Research Leader (No.17XD1400100), and the State Key Laboratory for Modification of Chemical Fibers and Polymer Materials (Donghua University).

References

[1] C. Fan, D. Wang, J. Huang, H. Ke, Q. Wei, A highly sensitive epidermal sensor based on triple-bonded hydrogels for strain/pressure sensing, Compos. Commun. 28 (2021) 100951.

[2] G. Wu, M. Panahi-Sarmad, X. Xiao, F. Ding, K. Dong, X. Hou, Fabrication of capacitive pressure sensor with extraordinary sensitivity and wide sensing range using PAM/BIS/GO nanocomposite hydrogel and conductive fabric, Composites, Part A 145 (2021) 106373.

[3] G. Zhu, P. Ren, J. Wang, Q. Duan, F. Ren, W. Xia, D. Yan, A highly sensitive and broad-range pressure sensor based on polyurethane mesodome arrays

embedded with silver nanowires, ACS Appl. Mater. Interfaces 12 (2020) 19988-19999.

[4] Y. Li, J. Xiong, J. Lv, J. Chen, D. Gao, X. Zhang, P.S. Lee, Mechanically interlocked stretchable nanofibers for multifunctional wearable triboelectric nanogenerator, Nano Energy 78 (2020) 105358.

[5] H. Kim, Y.-S. Kim, M. Mahmood, S. Kwon, F. Epps, Y.S. Rim, W.-H. Yeo, Wireless, continuous monitoring of daily stress and management practice via soft bioelectronics, Biosens. Bioelectron. 173 (2021) 112764.

[6] J.H. Kim, K.G. Cho, D.H. Cho, K. Hong, K.H. Lee, Ultra-sensitive and stretchable ionic skins for high-precision motion monitoring, Adv. Funct. Mater. 31 (2021) 2010199.

[7] Z. Wang, P. Bi, Y. Yang, H. Ma, Y. Lan, X. Sun, Y. Hou, H. Yu, G. Lu, L. Jiang, B. Zhu, R. Xiong, Star-nose-inspired multi-mode sensor for anisotropic motion monitoring, Nano Energy 80 (2021) 105559.

[8] G. Sang, P. Xu, T. Yan, V. Murugadoss, N. Naik, Y. Ding, Z. Guo, Interface engineered microcellular magnetic conductive polyurethane nanocomposite foams for electromagnetic interference shielding, Nano-Micro Lett. 13 (2021) 153.

[9] Q. Xia, S. Wang, W. Zhai, C. Shao, L. Xu, D. Yan, N. Yang, K. Dai, C. Liu, C. Shen, Highly linear and low hysteresis porous strain sensor for wearable electronic skins, Compos. Commun. 26 (2021) 100809.

[10] J. Zeng, W. Ma, Q. Wang, S. Yu, M.T. Innocent, H. Xiang, M. Zhu, Strong, high stretchable and ultrasensitive SEBS/CNTs hybrid fiber for high-performance strain sensor, Compos. Commun. 25 (2021) 100735.

[11] K. Zhang, L. Zheng, M.A. Aouraghe, F. Xu, Ultra-light-weight kevlar/polyimide 3D woven spacer multifunctional composites for high-gain microstrip antenna, Adv. Compos. Hybrid Mater. (2021) DOI: 10.1007/s42114-021-00382-2.

[12] H. Jin, M.O.G. Nayeem, S. Lee, N. Matsuhisa, D. Inoue, T. Yokota, D. Hashizume, T. Someya, Highly Durable Nanofiber-reinforced elastic conductors for skin-tight electronic textiles, ACS Nano 13 (2019) 7905-7912.

[13] Y. Chen, Z. Deng, R. Ouyang, R. Zheng, Z. Jiang, H. Bai, H. Xue, 3D printed stretchable smart fibers and textiles for self-powered e-skin, Nano Energy 84 (2021) 105866.

[14] H. Souri, H. Banerjee, A. Jusufi, N. Radacsi, A.A. Stokes, I. Park, M. Sitti, M. Amjadi, Wearable and stretchable strain sensors: materials, sensing mechanisms, and applications, Adv. Intell. Syst. 2 (2020) 2000039.

[15] H.J. Zhang, W.Q. Han, K. Xu, H.J. Lin, Y.F. Lu, H.D. Liu, R.Z. Li, Y.H. Du, Z.T. Nie, F. Xu, L. Miao, J.X. Zhu, W. Huang, Stretchable and ultrasensitive intelligent sensors for wireless human–machine manipulation, Adv. Funct. Mater. 31 (2021) 2009466.

[16] X. Chang, L. Chen, J. Chen, Y. Zhu, Z. Guo, Advances in transparent and stretchable strain sensors, Adv. Compos. Hybrid Mater. 4 (2021) 435-450.

[17] M. Fan, L. Wu, Y. Hu, M. Qu, S. Yang, P. Tang, L. Pan, H. Wang, Y. Bin, A highly stretchable natural rubber/buckypaper/natural rubber (NR/N-BP/NR) sandwich strain sensor with ultrahigh sensitivity, Adv. Compos. Hybrid Mater. 4 (2021) 1039-1047.

[18] L. Zhang, T. Song, L. Shi, N. Wen, Z. Wu, C. Sun, D. Jiang, Z. Guo, Recent progress for silver nanowires conducting film for flexible electronics, J. Nanostruct. Chem. 11 (2021) 323-341.

[19] S.u. Rehman, R. Ahmed, K. Ma, S. Xu, T. Tao, M.A. Aslam, M. Amir, J. Wang, Composite of Strip-shaped ZIF-67 with Polypyrrole: A conductive polymer-MOF electrode system for stable and high specific capacitance, Eng. Sci. 13 (2021) 71-78.

[20] S. Han Min, A.M. Asrulnizam, M. Atsunori, M. Mariatti, Properties of stretchable and flexible strain sensor based on silver/PDMS nanocomposites, Mater. Today: Proc. 17 (2019) 616-622.

[21] H. Yang, X. Xiao, Z. Li, K. Li, N. Cheng, S. Li, J.H. Low, L. Jing, X. Fu, S. Achavananthadith, F. Low, Q. Wang, P.-L. Yeh, H. Ren, J.S. Ho, C.-H. Yeow, P.-Y. Chen, Wireless $Ti_3C_2T_x$ MXene strain sensor with ultrahigh sensitivity and designated working windows for soft exoskeletons, ACS Nano 14 (2020) 11860-11875.

[22] X.H. Cui, Y. Jiang, Z.G. Xu, M. Xi, Y. Jiang, P.A. Song, Y. Zhao, H. Wang, Stretchable strain sensors with dentate groove structure for enhanced sensing recoverability, Composites, Part B 211 (2021) 108641.

[23] Y. Chen, L. Wang, Z.F. Wu, J.C. Luo, B. Li, X.W. Huang, H.G. Xue, J.F. Gao, Super-hydrophobic, durable and cost-effective carbon black/rubber composites for high performance strain sensors, Composites, Part B 176 (2019) 107358.

[24] Y. Niu, H. Liu, R.Y. He, Z.D. Li, H. Ren, B. Gao, H. Guo, G.M. Genin, F. Xu, The new generation of soft and wearable electronics for health monitoring in varying environment: From normal to extreme conditions, Mater. Today 41 (2020) 219-242.

[25] Z. Li, M. Cao, P. Li, Y. Zhao, H. Bai, Y. Wu, L. Jiang, Surface-embedding of functional micro-/nanoparticles for achieving versatile superhydrophobic interfaces, Matter 1 (2019) 661-673.

[26] C. Peng, Z. Chen, M.K. Tiwari, All-organic superhydrophobic coatings with mechanochemical robustness and liquid impalement resistance, Nat. Mater. 17 (2018) 355-360.

[27] Y. Liu, L. Zhao, J. Lin, S. Yang, Electrodeposited surfaces with reversibly switching interfacial properties, Sci. Adv. 5 (2019) eaax0380.

[28] Y. Lu, S. Sathasivam, J. Song, C.R. Crick, C.J. Carmalt, I.P. Parkin, Robust self-cleaning surfaces that function when exposed to either air or oil, Science 347 (2015) 1132.

[29] L. Li, Y. Bai, L. Li, S. Wang, T. Zhang, A superhydrophobic smart coating for flexible and wearable sensing electronics, Adv. Mater. 29 (2017) 1702517.

[30] H. Liu, Q. Li, Y. Bu, N. Zhang, C. Wang, C. Pan, L. Mi, Z. Guo, C. Liu, C. Shen, Stretchable conductive nonwoven fabrics with self-cleaning capability for tunable wearable strain sensor, Nano Energy 66 (2019) 104143.

[31] Z. Dai, S. Ding, M. Lei, S. Li, Y. Xu, Y. Zhou, B. Zhou, A superhydrophobic and anti-corrosion strain sensor for robust underwater applications, J. Mater. Chem. A 9 (2021) 15282-15293.

[32] F. Qiang, L.-L. Hu, L.-X. Gong, L. Zhao, S.-N. Li, L.-C. Tang, Facile synthesis of super-hydrophobic, electrically conductive and mechanically flexible functionalized graphene nanoribbon/polyurethane sponge for efficient oil/water separation at static and dynamic states, Chem. Eng. J. 334 (2018) 2154-2166.

[33] P. Wang, X. Zhang, W. Duan, W. Teng, Y. Liu, Q. Xie, Superhydrophobic flexible supercapacitors formed by integrating hydrogel with functional carbon nanomaterials, Chin. J. Chem. 39 (2021) 1153-1158.

[34] X. Li, J. Liu, R. Qu, W. Zhang, Y. Liu, H. Zhai, Y. Wei, H. Hu, L. Feng, Universal and tunable liquid–liquid separation by nanoparticle-embedded gating membranes based on a self-defined interfacial parameter, Nat. Commun. 12 (2021) 80.

[35] C.M. De León-Almazán, I.A. Estrada-Moreno, J.L. Olmedo-Martínez, J.L. Rivera-Armenta, Semiconducting elastomers based on polyaniline/clay nanocomposites and SEBS obtained by an alternative processing technique, Synth. Met. 268 (2020) 116460.

[36] D.M. Chipara, D.M. Panaitescu, K. Lozano, R.A. Gabor, C.A. Nicolae, M. Chipara, Raman spectroscopy and molecular bases of elasticity: SEBS-graphite composites, Polymer 176 (2019) 74-88.

[37] L. Lin, L. Wang, B. Li, J. Luo, X. Huang, Q. Gao, H. Xue, J. Gao, Dual conductive network enabled superhydrophobic and high performance strain sensors with outstanding electro-thermal performance and extremely high gauge factors, Chem. Eng. J. 385 (2020) 123391.

[38] M.R. Bockstaller, R.A. Mickiewicz, E.L. Thomas, Block copolymer nanocomposites: perspectives for tailored functional materials, Adv. Mater. 17 (2005) 1331-1349.

[39] I. You, M. Kong, U. Jeong, Block copolymer elastomers for stretchable electronics, Acc. Chem. Res. 52 (2019) 63-72.

[40] J. Dong, L. Li, C. Zhang, P. Ma, W. Dong, Y. Huang, T. Liu, Ultra-highly stretchable and anisotropic SEBS/F127 fiber films equipped with an adaptive deformable carbon nanotube layer for dual-mode strain sensing, J. Mater. Chem. A 9 (2021) 18294-18305.

[41] R. Chen, X. Xu, D. Yu, C. Xiao, M. Liu, J. Huang, T. Mao, C. Zheng, Z. Wang, X. Wu, Highly stretchable and fatigue resistant hydrogels with low Young's modulus as transparent and flexible strain sensors, J. Mater. Chem. C 6 (2018) 11193-11201.

[42] F. Stauffer, Q. Zhang, K. Tybrandt, B. Llerena Zambrano, J. Hengsteler, A. Stoll, C. Trüeb, M. Hagander, J.-M. Sujata, F. Hoffmann, J. Schuurmans Stekhoven, J. Quack, H. Zilly, J. Goedejohann, M.P. Schneider, T.M. Kessler, W.R. Taylor, R. Küng, J. Vörös, Soft electronic strain sensor with chipless wireless readout: toward real-time monitoring of bladder volume, Adv. Mater. Technol. 3 (2018) 1800031.

[43] M.N. Ren, Y. Zhou, Y. Wang, G.Q. Zheng, K. Dai, C.T. Liu, C.Y. Shen, Highly stretchable and durable strain sensor based on carbon nanotubes decorated thermoplastic polyurethane fibrous network with aligned wave-like structure, Chem. Eng. J. 360 (2019) 762-777.

[44] H. Yu, J. Li, G. Chen, R. Zhang, Y. Li, B. Qiu, X. Li, Effects of phosphate emulsion-based montmorillonite on structure and properties of poly(styrene-ethylene-butylene-styrene) triblock copolymer, Polym. Eng. Sci. 60 (2020) 1343-1352.

[45] M. Fu, J.M. Zhang, Y.M. Jin, Y. Zhao, S.Y. Huang, C.F. Guo, A highly sensitive, reliable, and high-temperature-resistant flexible pressure sensor based on ceramic nanofibers, Adv. Sci. 7 (2020) 2000258.

[46] J. Xu, R. Jing, X. Ren, G. Gao, Fish-inspired anti-icing hydrogel sensors with low-temperature adhesion and toughness, J. Mater. Chem. A 8 (2020) 9373-9381.

[47] X. Sun, Z. Qin, L. Ye, H. Zhang, Q. Yu, X. Wu, J. Li, F. Yao, Carbon nanotubes reinforced hydrogel as flexible strain sensor with high stretchability and mechanically toughness, Chem. Eng. J. 382 (2020) 122832.

[48] R. Blossey, Self-cleaning surfaces-virtual realities, Nat. Mater. 2 (2003) 301-306.

[49] D. Yoo, Y. Kim, M. Min, G.H. Ahn, D.-H. Lien, J. Jang, H. Jeong, Y. Song, S. Chung, A. Javey, T. Lee, Highly reliable superhydrophobic protection for organic field-effect transistors by fluoroalkylsilane-coated TiO_2 nanoparticles, ACS Nano 12 (2018) 11062-11069.

[50] X. Deng, L. Mammen, H.-J. Butt, D. Vollmer, Candle soot as a template for a transparent robust superamphiphobic coating, Science 335 (2012) 67.

[51] S. Cho, D.-h. Kang, H. Lee, M.P. Kim, S. Kang, R. Shanker, H. Ko, Highly stretchable sound-in-display electronics based on strain-insensitive metallic nanonetworks, Adv. Sci. 8 (2021) 2001647.

[52] Y. Cheng, X. Xiao, K. Pan, H. Pang, Development and application of self-healing materials in smart batteries and supercapacitors, Chem. Eng. J. 380 (2020) 122565.

[53] S. Yang, Y. Cheng, X. Xiao, H. Pang, Development and application of carbon fiber in batteries, Chem. Eng. J. 384 (2020) 123294.

[54] X. Zhao, H. Chen, F. Kong, Y. Zhang, S. Wang, S. Liu, L.A. Lucia, P. Fatehi, H. Pang, Fabrication, characteristics and applications of carbon materials with different morphologies and porous structures produced from wood liquefaction: A review, Chem. Eng. J. 364 (2019) 226-243.

[55] Y.-L. Zhang, Y.-Y. Zheng, Z.-C. Ma, Y.-N. Sun, Radial pulse transit time is an index of arterial stiffness, Hypertens. Res. 34 (2011) 884-887.

[56] K. Kohara, Y. Tabara, A. Oshiumi, Y. Miyawaki, T. Kobayashi, T. Miki, Radial augmentation index: A useful and easily obtainable parameter for vascular aging, Am. J. Hypertens. 18 (2005) 11S-14S.